

Quantum Anomalous Hall Effect in Antiferromagnetism

Peng-Jie Guo,^{1,*} Zheng-Xin Liu,^{1,†} and Zhong-Yi Lu^{1,‡}

¹*Department of Physics and Beijing Key Laboratory of Opto-electronic Functional Materials & Micro-nano Devices, Renmin University of China, Beijing 100872, China*

(Dated: June 8, 2022)

So far, experimentally realized quantum anomalous Hall (QAH) insulators all exhibit ferromagnetic order and the QAH effect only occurs at very low temperatures. On the other hand, up to now the QAH effect in antiferromagnetic (AFM) materials has never been reported. In this letter, we realize the QAH effect by proposing a four-band lattice model with static AFM order, which indicates that the QAH effect can be found in AFM materials. Then, as a prototype, we demonstrate that a monolayer CrO can be switched from an AFM Weyl semimetal to an AFM QAH insulator by applying strain, based on symmetry analysis and the first-principles electronic structure calculations. Our work not only proposes a new scenario to search for QAH insulators in materials, but also reveals a way to considerably increase the critical temperature of the QAH phase.

Introduction. Anomalous Hall effect, which exists in ferromagnetic metals[1, 2], means that the electric Hall conductance remains to be finite even at zero external magnetic field. Furthermore, if the system becomes insulating, the Hall conductance is quantized to an integer C times e^2/h with C being the Chern number of its band structure. This effect is called the quantum anomalous Hall (QAH) effect. QAH insulators, i.e. magnetic insulators exhibiting QAH effect ($C \neq 0$), as important members in the family of quantum Hall systems, have attracted intensive interest from both theoretical and experimental physicists [3–8]. In 1988, Haldane proposed a lattice model of spinless fermions to realize integer Hall effect in a staggered magnetic flux with zero net magnetic field[9]. Later it was proposed that ferromagnetic insulators with spin-orbit coupling (SOC) may exhibit QAH effect [4, 10]. And there was also an attempt to derive AFM Chern insulator from the Kane-Mele Hubbard model [11]. Meanwhile, many materials have been predicted to be QAH insulators[12–26]. So far, QAH effect has been experimentally observed in four different classes of two-dimensional (2D) systems: thin films of magnetically doped topological insulators[27], thin films of the intrinsic magnetic topological insulators[28], moiré materials formed from graphene[29], and transition metal dichalcogenides[30]. In all of these materials, the QAH plateau only shows up at very low temperatures (of order of 1 Kelvin or lower).

It was believed that ferromagnetism is necessary for experimental realization of QAH effect[4]. However, ferromagnetism can be found easily in metals but rarely in insulators. For this reason, the critical temperature of the observed QAH phase is very low. On the other hand, there are plenty of AFM insulating materials in nature even above room temperatures. However, so far the QAH effect has never been found in AFM materials, even the corresponding mechanism has never been proposed. Supposing that it can be realized in AFM insulators (especially those containing collinear AFM order), then the realization of QAH effect will be much cheaper.

Attractively, the critical temperature for observing the QAH effect may be greatly increased since the critical temperature of the AFM order can be very high. The resultant AFM QAH insulators can have extensive applications in designing devices. Therefore, the realization of QAH effect in AFM materials is a very important issue both academically and practically.

Collinear antiferromagnetic (AFM) systems usually possess an ‘effective time-reversal’ symmetry such as $\{\mathcal{T}|\tau\}$ or \mathcal{IT} , where \mathcal{T} stands for the time reversal operation, τ denotes the associated fractional translation, and \mathcal{I} represents the spatial inversion. Such an ‘effective time-reversal’ symmetry restricts the Chern number of a gapped ground state to be $C = 0$, resulting in a trivial band insulator. This limits the study of QAH effect in collinear AFM systems. However, not all collinear AFM systems have the ‘effective time-reversal’ symmetry. Exceptions include the systems having type-I or some of the type-III magnetic space groups. QAH effect can be possibly realized in these collinear AFM insulators.

In this letter, we propose a four-band lattice model to realize QAH effect in a collinear AFM insulator. Furthermore, based on symmetry analysis and the first-principles electronic structure calculations, we illustrate that a monolayer CrO is a collinear AFM semimetal with C_{2v} symmetry protected Weyl cones. And we further show that by applying external strain to lower its point group symmetry, the monolayer CrO can open a gap and be turned into an AFM QAH insulator.

Lattice model. We firstly consider a square lattice with two sites (labeled by sublattice index $\alpha = 1, 2$) in each unit cell which contains local anti-parallel magnetic moments $\mathbf{m}_1 = -\mathbf{m}_2 = \mathbf{m}$. The tight-binding model for

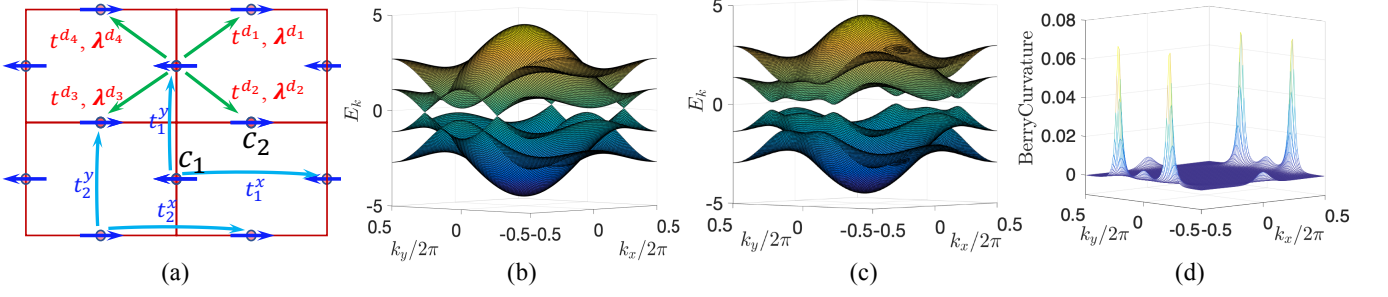


FIG. 1. Model for the AFM QAH insulator. (a) illustration of the Hamiltonian in Eq. (1); (b) without SOC the ground state being a Weyl semimetal with a pair of Weyl cones on the (π, k_y) boundary of the BZ; (c) with SOC the band structure being gapped with Chern number $C = 1$; (d) the Berry curvature which is inversion symmetric.

spin-orbit coupled electrons in the lattice reads

$$\begin{aligned}
 H = & \sum_{j, d_i} \left[t^{d_i} C_{1,j}^\dagger C_{2,j+d_i} + C_{1,j}^\dagger (i\lambda^{d_i} \cdot \boldsymbol{\sigma}) C_{2,j+d_i} + \text{h.c.} \right] \\
 & + \sum_{\alpha, j} \left[t_\alpha^x C_{\alpha, j}^\dagger C_{\alpha, j+\mathbf{x}} + t_\alpha^y C_{\alpha, j}^\dagger C_{\alpha, j+\mathbf{y}} + \text{h.c.} \right] \\
 & + \sum_{\alpha, j} C_{\alpha, j}^\dagger [\mu_\alpha \sigma_0 + \mathbf{m}_\alpha \cdot \boldsymbol{\sigma}] C_{\alpha, j}, \quad (1)
 \end{aligned}$$

where $C_{\alpha, j}^\dagger = (c_{\alpha, j\uparrow}^\dagger, c_{\alpha, j\downarrow}^\dagger)$ are electron creation operators, t^{d_i} and t_α^x, t_α^y are the kinetic hopping terms along $\mathbf{d}_{1,2,3,4}$ and \mathbf{x}, \mathbf{y} directions respectively, with $\mathbf{x} = a_1 \hat{x}, \mathbf{y} = a_2 \hat{y}$, a_1, a_2 being the lattice constants and \hat{x}, \hat{y} being unit vectors, and $\mathbf{d}_{1,3} = \pm \frac{1}{2}(\mathbf{x} + \mathbf{y}), \mathbf{d}_{2,4} = \pm \frac{1}{2}(\mathbf{x} - \mathbf{y})$. The $i\lambda^{d_i} \cdot \boldsymbol{\sigma}$ term denotes spin-orbit coupling, $\mathbf{m}_\alpha = (-1)^\alpha \mathbf{m}$ stands for the static collinear AFM order which couples to the electron spin as a Zeeman field, and μ_α represents the chemical potential on the α -sublattice. We further define $\mu_\pm = \frac{1}{2}(\mu_1 \pm \mu_2)$, where μ_- is the staggered potential energy and μ_+ is adopted such that the energy bands are half-filled. Here we ignore the correlation between the electrons by simply assuming that the AFM moment couples to the electron spin as a Zeeman field. The effect of electron correlations, such as the Anderson or the Kondo coupling terms, will be left for future study.

Since inversion symmetry is crucial to guarantee a nonzero Chern number, it requires that $t^{d_1} = t^{d_3}, t^{d_2} = t^{d_4}$ and $\lambda^{d_1} = \lambda^{d_3}, \lambda^{d_2} = \lambda^{d_4}$. For simplicity, we set $t^{d_1} = t^{d_2} = t^d$ and $\lambda^{d_1} = -\lambda^{d_2} = \boldsymbol{\lambda}$. Furthermore, to ensure that the energy bands have a full gap, we let $t_\alpha^{x,y} = (-1)^\alpha t^{x,y}$. After the Fourier transformation, the above Hamiltonian can be rewritten in momentum space as

$$H = \sum_k (C_{1k}^\dagger \Gamma_k^{12} C_{2k} + \text{h.c.}) + \sum_{\alpha, k} C_{\alpha k}^\dagger \Gamma_k^{(\alpha)} C_{\alpha k}, \quad (2)$$

with $C_{\alpha k}^\dagger = (c_{\alpha k\uparrow}^\dagger, c_{\alpha k\downarrow}^\dagger)$ the fermion operators, $\Gamma_k^{12} = 2(t^d + i\boldsymbol{\lambda} \cdot \boldsymbol{\sigma}) \cos(\frac{k_x}{2} + \frac{k_y}{2}) + 2(t^d - i\boldsymbol{\lambda} \cdot \boldsymbol{\sigma}) \cos(\frac{k_x}{2} - \frac{k_y}{2})$ the inter-sublattice terms and $\Gamma_k^{(\alpha)} = (-1)^\alpha 2(t^x \cos k_x + t^y \cos k_y) + (\mu_\alpha + \mathbf{m}_\alpha \cdot \boldsymbol{\sigma})$ the intra-sublattice terms.

We firstly turn off the SOC by setting $\lambda^{d_1} = \lambda^{d_2} = 0$, then the system has a spin point group symmetry[31–34] generated by $(E||C_2^z), (E||C_2^x), (E||\mathcal{I})$ and $(C_2^\perp \mathcal{T}||\mathcal{T}), (C_2^m||E)$, where the notation $(g||h)$ denotes a combined operation of the spin operation g and the lattice operation h , and C_2^\perp/C_2^m respectively stand for the 2-fold spin rotation along the axis perpendicular/parallel to the \mathbf{m} -direction. In this case the Γ_k^{12} term vanishes on the boundary of the BZ. In other words, the two species of fermions C_{1k} and C_{2k} do not hybridize if $k_x = \pi$ or $k_y = \pi$. It can be shown that on the boundary line (k_x, π) , the C_{1k}, C_{2k} bands carry quantum numbers 1 and -1 of the symmetry operation $(E||C_2^x)$ [or $(E||M_y)$], respectively. Similarly, on the line (π, k_y) the C_{1k}, C_{2k} bands respectively carry quantum numbers -1 and 1 of the symmetry operation $(E||C_2^y)$ [or $(E||M_x)$]. Owing to these different quantum numbers, if the C_{1k} and C_{2k} bands are inverted, the band crossing will be protected from opening a gap. Resultantly, on the boundary lines (k_x, π) and/or (π, k_y) there will be pairs of Weyl cones (see Fig.1(b) as an example) among which the two in each pair are related by the inversion \mathcal{I} operation. It can be further shown that when the condition (4) given below is satisfied, there will be odd pairs of Weyl cones on the BZ boundary [see the Supplemental Materials [35](SM)]. In the SM we also show that the Weyl cones are robust under perturbations as long as the symmetry $(E||\mathcal{I}) \times (C_2^\perp \mathcal{T}||\mathcal{T}) = (C_2^\perp \mathcal{T}||\mathcal{I}\mathcal{T})$ is unbroken.

Then we turn on the SOC. In this case, the physical symmetry is described by a magnetic point group owing to the locking of the lattice rotation g and the spin rotation g (we will simply denote $(g||g)$ as g in the following). Generally, if $\boldsymbol{\lambda} \cdot \mathbf{m} \neq 0$ then all the Weyl cones obtain a mass and the energy band is fully gapped (see Fig.1(c)). Noticing that the SOC does not break the inversion symmetry \mathcal{I} , and that the pattern of the Berry curvature of the occupied bands is invariant under \mathcal{I} (see Fig.1(d)), each pair of Weyl cones (related by \mathcal{I}) together contribute either 1 or -1 to the total Chern number (recalling that a single cone carries a π Berry phase or $\pm 1/2$ Chern number). Therefore, if there are an odd number

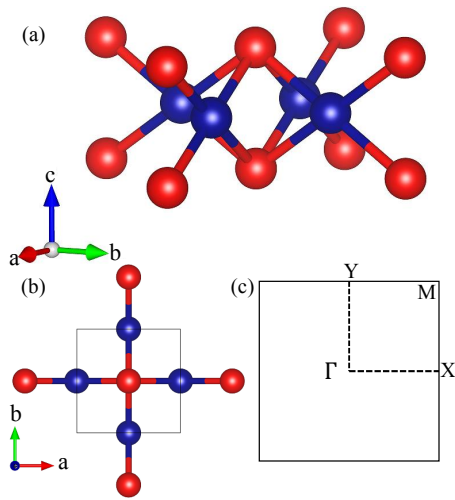


FIG. 2. Crystal structure of the monolayer CrO viewed along (a) [110] and (b) [001] directions. (c) The Brillouin zone and the corresponding high-symmetry points. The red and blue balls represent the O and Cr atoms, respectively.

of pairs of Weyl cones, the Chern number in the gapped state must be nonzero and the system will exhibit QAH effect.

The conditions for the nontrivial total Chern number (± 1) can be summarized as the following inequalities,

$$t^d \neq 0, \quad \boldsymbol{\lambda} \cdot \mathbf{m} \neq 0, \quad (3)$$

$$\left| |\mathbf{m}| - 2|t^y - t^x| \right| < |\mu_-| < |\mathbf{m}| + 2|t^y - t^x|. \quad (4)$$

These conditions restrict the crystalline symmetry of the potential materials (see SM for detailed discussions). If the AFM order lies in the lattice plane (without loss of generality we assume $\mathbf{m} \parallel \hat{y}$), then the QAH effect can be realized in triclinic lattice with symmetry $\bar{1} = \{E, \mathcal{I}\}$ or monoclinic lattice with magnetic point group $2'/m' = \{E, \mathcal{I}, C_2^x \mathcal{T}, M_x \mathcal{T}\}$. On the other hand, if the AFM order is perpendicular to the lattice plane (namely $\mathbf{m} \parallel \hat{z}$), then the conditions (3) and (4) can be satisfied in orthogonal lattice with magnetic point group symmetry $m'm'm = \{E, C_2^x \mathcal{T}, C_2^y \mathcal{T}, C_2^z, \mathcal{I}, M_x \mathcal{T}, M_y \mathcal{T}, M_z\}$.

If $\boldsymbol{\lambda} \cdot \mathbf{m} = 0$, and if \mathbf{m} lies in the lattice plane, e.g. $\mathbf{m} \parallel y$, then the $(C_2^y || C_2^y)$ or the $(C_2^y || M_y) = (C_2^y || C_2^y) \times (E || \mathcal{I})$ symmetry can protect the Weyl cones on the BZ boundary from being gapped out (see SM). This means that if the AFM order is parallel to an in-plane C_2 axis, then the QAH effect cannot be realized through our mechanism.

Now we stress that the spin-orbit coupling term in model (1) is inversion symmetric. When $\boldsymbol{\lambda}^{d_1} = \lambda \hat{x}$, $\boldsymbol{\lambda}^{d_2} = \lambda \hat{y}$, it looks like a Rashba SOC term, but the difference is that the Rashba term breaks \mathcal{I} symmetry while our model (1) does not. In this case, the QAH effect can be realized if conditions $\mathbf{m} \cdot (\hat{x} + \hat{y}) \neq 0$ and (4) are satisfied.

It is interesting to compare the model (1) with the Haldane model[9] and the FM QAH model[10]. Without

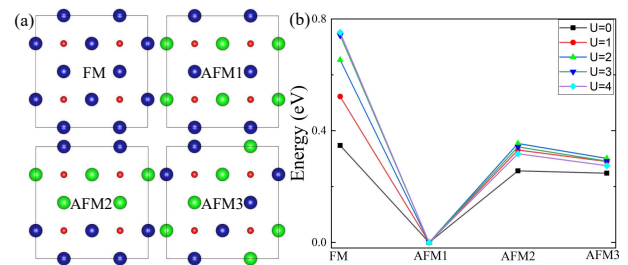


FIG. 3. (a) Cartoon pictures for four possible magnetic structures of a monolayer CrO, where FM and AFM represent ferromagnetism and antiferromagnetism, respectively. The blue and green balls represent Cr atoms with opposite spin. (b) The relative energies (per Cr atom) of the four ordered states under different Hubbard U (eV).

introducing external magnetic fields, all of these models have a gapped ground state with a nonzero Chern number. In the Haldane model, a staggered flux is needed in which the fermions obtain the Aharonov-Bohm phase. Although the total flux is zero, a staggered flux is not easy to implement in practice. In the FM QAH model, the staggered flux is replaced by the Berry phase resulting from spin-orbit coupling, and the role of the FM order is to polarize the spin of the electrons. However, the FM critical temperature in insulators is generally very low. In our model, the AFM order provides a local Zeeman field for the electrons, the SOC and the sub-lattice dependent chemical potentials guarantee a full gap and a nontrivial Chern number. The advantage is that the AFM critical temperature can be very high (even with an order of 1000 Kelvin). Therefore, if the band gap is not too small, then hopefully the QAH effect can be realized in experiments close to room temperatures.

As discussed above, the low-energy effective model (1) reveals the possibility that QAH effect can exist in AFM insulators. In the following, by studying a concrete material as a prototype — a monolayer CrO, we illustrate that QAH effect can indeed be obtained in AFM materials.

Candidate Material. A monolayer CrO has a square lattice structure whose symmetry is described by the symmorphic space group P4-mmm. The point group of P4-mmm is D_{4h} generated by C_4^z, C_2^x and \mathcal{I} . The unit cell of a monolayer CrO contains two O atoms plus two Cr atoms (see Fig.2 (a) and (b)) and the corresponding BZ is shown in Fig.2 (c). The Cr^{2+} ions have a fairly strong correlation and they interact with each other via super-exchange interactions mediated by the O atoms. It was suggested in Ref.[36] that monolayer CrO is in antiferromagnetic phase with a high Neel temperature.

To confirm the magnetic structure of a monolayer CrO, we compare the energies of four trial states with different magnetic orders under different Hubbard U . As shown in Fig.3(a), indeed the AFM1 state (i.e. the collinear Neel state) is always lowest in energy. Notice that the AFM1

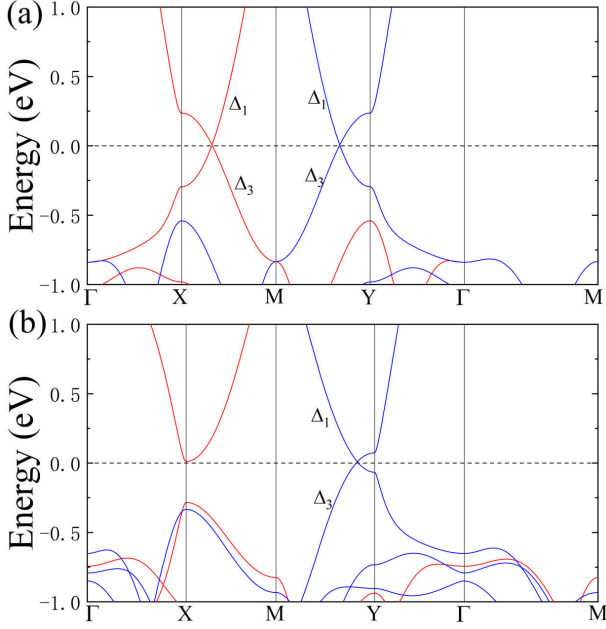


FIG. 4. The band structure of monolayer CrO along the high-symmetry directions, (a) no SOC, (b) no SOC, but tensile strain 10 percent along b direction. The spin-up and spin-down bands in (a) and (b) are marked in red and blue, respectively. The Δ_1 and Δ_3 represent different irreducible representations of the little co-group C_{2v} .

order has no ‘effective time-reversal symmetry’ like \mathcal{IT} or $\{\mathcal{T}|\tau\}$. Furthermore, since the electronic band structure is sensitive to the Hubbard U , we need to determine the proper value of U . By comparing the electronic band structure of Heyd-Scuseria-Ernzerhof (HSE) hybrid functional within the framework of HSE06[37], we find that $U = 3.2$ eV, which is slightly less than 3.5 eV as proposed in [36]. This is due to the fact that our relaxed lattice parameter is 1.4 percent less than that adopted in [36].

When ignoring the SOC, a monolayer CrO has a spin point group symmetry whose generators are $(\mathcal{T}|\mathcal{TC}_4^z)$, $(E||M_z)$, $(E||M_x)$, $(\mathcal{T}|\mathcal{TM}_{x+y})$ and $(C_2^{\perp}\mathcal{T}|\mathcal{T})$, $(C_2^m||E)$. According to the $(\mathcal{T}|\mathcal{TC}_2^{x\pm y}) = (E||M_z)(\mathcal{T}|\mathcal{TM}_{x\mp y})$ symmetry, the spin-up and spin-down are degenerate on the high-symmetry lines Γ - M along the $x + y$ or $x - y$ direction. Away from these two high symmetry lines, the spin degeneracy is generally lifted as illustrated in Fig.4(a), where the red and blue lines represent spin-up and spin-down bands, respectively. Furthermore, the band inversion occurs around the X and Y points which are related to each other by the $(\mathcal{T}|\mathcal{TC}_4^z)$ symmetry and hence carry opposite spins. Since the two inverted bands carry different quantum numbers of $(E||C_2^x)$ or $(E||C_2^y)$, the band inversion results in a band crossing with two pairs of Weyl points[36]. The two pairs of Weyl cones around the X,Y points can also appear in the model (1) when $t^x = t^y$ and $\lambda = 0$.

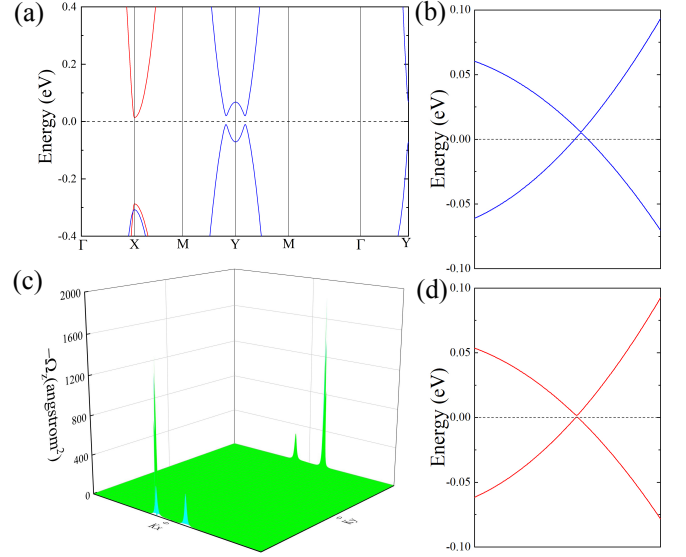


FIG. 5. The Weyl cones of a monolayer CrO shift their positions from the M-Y high symmetry line to the inside of the BZ by the tensile and shear strain, and are further gaped out if SOC is turned on. (a) & (b) show the electronic band structure (with strain and without SOC) along the M-Y line and the line $k_y = 0.49747 \times \frac{2\pi}{a_2}$ respectively, it can be seen that the Weyl points shift toward the inside of the BZ. (c) & (d) respectively show the Berry curvature and the dispersion (around the Weyl point) of the gapped bands when SOC is turned on.

If the $(\mathcal{T}|\mathcal{TC}_4^z)$ symmetry is preserved, then after the two pairs of Weyl cones being gapped out, the Berry curvature contributed from these cones will exactly cancel each other, resulting in a trivial Chern number. Therefore, in order to realize the QAH effect in a monolayer CrO, the $(\mathcal{T}|\mathcal{TC}_4^z)$ symmetry must be removed. To this end, we apply a tensile strain 10 percent along the b-direction. Then the crystalline point group of the strained monolayer CrO reduces to D_{2h} which is generated by C_2^z, C_2^x and \mathcal{I} .

Under the above tensile strain, the calculated electronic band structure is shown in Fig.4(b), where the pair of Weyl points on the X-M axis merge and gap out with the disappearing of band inversion. But the pair of Weyl points on the Y-M axis remain stable. When considering the SOC, our calculations indicate that the magnetic moments are along the \hat{y} -direction in the lattice plane. Then the monolayer CrO has a magnetic point group symmetry $m'mm' = \{E, C_2^x\mathcal{T}, C_2^y, C_2^z\mathcal{T}, \mathcal{I}, M_x\mathcal{T}, M_y, M_z\mathcal{T}\}$ However, due to the $C_2^z\mathcal{T} \equiv (C_2^z\mathcal{T}||C_2^z\mathcal{T})$ symmetry, the Berry curvature is always zero in the whole BZ and the Weyl cones are still robust. Therefore, the $C_2^z\mathcal{T}$ symmetry has to be removed to gap out the Weyl cones and then to realize the QAH effect.

To break the $C_2^z\mathcal{T}$ symmetry, we further apply shear strain (up to 3 percent) such that the two out-of-plane O atoms obtain a slight displacement along the in-plane di-

agonal direction (the inversion symmetry is always kept). At this time, the monolayer CrO has only space-inversion symmetry \mathcal{I} . Finally, the pair of Weyl cones open a gap for amount ~ 1 meV (see Fig.5(d) for the gapped cone) and the resultant gapped ground state has a Chern number $C = -1$, which makes the strained monolayer CrO a QAH insulator. As shown in Fig.5(c), the Berry curvature mainly concentrates around the gapped Weyl points.

It should be emphasized that SOC plays an important role in giving mass to the Weyl cones. If SOC is absent, the Weyl cones are robust against the strains [see Fig.5(a)&(b) where the Weyl points on the Y-M line shift to (0.09025, 0.49747) and (-0.09025, -0.49747)] owing to the protection of the spin point group symmetry element ($C_2^z \mathcal{T} || \mathcal{IT}$). So it is not a wonder that the size of the gap is rather small since the SOC in CrO is very weak. For this reason, the QAH effect can only be observed at about 10 Kelvin even though the Neel temperature of a monolayer CrO is estimated to be above the room temperature[36].

As mentioned, the monolayer CrO is just a prototype to demonstrate the mechanism of realizing QAH effect in an AFM system. The critical temperature of QAH effect can be promisingly enhanced in other candidate materials with stronger SOC. We believe that our work will arouse further interest in the study of QAH effect in AFM systems.

In summary, we come up with a four-band lattice model to illustrate that QAH effect can exist in antiferromagnetism. Furthermore, we predict that the monolayer CrO is a candidate AFM material to realize the QAH effect. Based on symmetry analysis and the first-principles electronic structure calculations, we first show that a monolayer CrO is an AFM semimetal containing Weyl cones. Then we demonstrate that by adding tensile and shear stain, the monolayer CrO can be turned into an AFM QAH insulator. Our study reveals a new scenario to realize QAH insulator in AFM materials. Especially, once QAH insulator is realized in AFM systems with strong SOC, it may allow people to observe QAH effect close to room temperatures.

Acknowledgments. We thank J.-W. Liu, C.-C. Liu, X.-H. Kong, Z.-M. Yu for valueable discussions. This work was financially supported by the NSF of China (No. 12134020, No. 11974421 and No. 11934020).

* guopengjie@ruc.edu.cn

† liuzxphys@ruc.edu.cn

‡ zlu@ruc.edu.cn

- [1] T. Jungwirth, Q. Niu, and A. H. MacDonald, Anomalous hall effect in ferromagnetic semiconductors, *Phys. Rev. Lett.* **88**, 207208 (2002).
 [2] N. Nagaosa, J. Sinova, S. Onoda, A. H. MacDonald, and N. P. Ong, Anomalous hall effect, *Rev. Mod. Phys.* **82**,

1539 (2010).

- [3] H. Weng, R. Yu, X. Hu, X. Dai, and Z. Fang, Quantum anomalous hall effect and related topological electronic states, *Advances in Physics* **64**, 227 (2015), <https://doi.org/10.1080/00018732.2015.1068524>.
 [4] C.-X. Liu, S.-C. Zhang, and X.-L. Qi, The quantum anomalous hall effect: Theory and experiment, *Annual Review of Condensed Matter Physics* **7**, 301 (2016), <https://doi.org/10.1146/annurev-conmatphys-031115-011417>.
 [5] C.-Z. Chang and M. Li, *J. Phys.: Condens. Matter* **28**, 123002 (2016).
 [6] K. He, Y. Wang, and Q.-K. Xue, Topological materials: Quantum anomalous hall system, *Annual Review of Condensed Matter Physics* **9**, 329 (2018), <https://doi.org/10.1146/annurev-conmatphys-033117-054144>.
 [7] Y. Tokura, K. Yasuda, and A. Tsukazaki, Magnetic topological insulators, *Nature Reviews Physics* **1**, 126 (2019).
 [8] C.-Z. Chang, C.-X. Liu, and A. H. MacDonald, *ArXiv: 2202*, 13902 (2022).
 [9] F. D. M. Haldane, Model for a quantum hall effect without landau levels: Condensed-matter realization of the "parity anomaly", *Phys. Rev. Lett.* **61**, 2015 (1988).
 [10] X.-L. Qi, Y.-S. Wu, and S.-C. Zhang, Topological quantization of the spin hall effect in two-dimensional paramagnetic semiconductors, *Phys. Rev. B* **74**, 085308 (2006).
 [11] K. Jiang, S. Zhou, X. Dai, and Z. Wang, Antiferromagnetic chern insulators in noncentrosymmetric systems, *Phys. Rev. Lett.* **120**, 157205 (2018).
 [12] C.-X. Liu, X.-L. Qi, X. Dai, Z. Fang, and S.-C. Zhang, Quantum anomalous hall effect in $\text{Hg}_{1-y}\text{Mn}_y\text{Te}$ quantum wells, *Phys. Rev. Lett.* **101**, 146802 (2008).
 [13] R. Yu, W. Zhang, H.-J. Zhang, S.-C. Zhang, X. Dai, and Z. Fang, Quantized anomalous hall effect in magnetic topological insulators, *Science* **329**, 61 (2010).
 [14] Z. F. Wang, Z. Liu, and F. Liu, Quantum anomalous hall effect in 2d organic topological insulators, *Phys. Rev. Lett.* **110**, 196801 (2013).
 [15] C. Fang, M. J. Gilbert, and B. A. Bernevig, Large- Chern-number quantum anomalous hall effect in thin-film topological crystalline insulators, *Phys. Rev. Lett.* **112**, 046801 (2014).
 [16] S.-C. Wu, G. Shan, and B. Yan, Prediction of near-room-temperature quantum anomalous hall effect on honeycomb materials, *Phys. Rev. Lett.* **113**, 256401 (2014).
 [17] Y. Ren, J. Zeng, X. Deng, F. Yang, H. Pan, and Z. Qiao, Quantum anomalous hall effect in atomic crystal layers from in-plane magnetization, *Phys. Rev. B* **94**, 085411 (2016).
 [18] C. Huang, J. Zhou, H. Wu, K. Deng, P. Jena, and E. Kan, Quantum anomalous hall effect in ferromagnetic transition metal halides, *Phys. Rev. B* **95**, 045113 (2017).
 [19] P. Chen, J.-Y. Zou, and B.-G. Liu, Intrinsic ferromagnetism and quantum anomalous hall effect in a cobr2 monolayer, *Phys. Chem. Phys.* **19**, 13432 (2017).
 [20] J.-Y. You, Z. Zhang, B. Gu, and G. Su, Two-dimensional room-temperature ferromagnetic semiconductors with quantum anomalous hall effect, *Phys. Rev. Applied* **12**, 024063 (2019).
 [21] F. Wu, T. Lovorn, E. Tutuc, I. Martin, and A. H. MacDonald, Topological insulators in twisted transition metal dichalcogenide homobilayers, *Phys. Rev. Lett.* **122**, 086402 (2019).

- [22] D. Zhang, M. Shi, T. Zhu, D. Xing, H. Zhang, and J. Wang, Topological axion states in the magnetic insulator mnbi_2te_4 with the quantized magnetoelectric effect, *Phys. Rev. Lett.* **122**, 206401 (2019).
- [23] Y.-H. Zhang, D. Mao, and T. Senthil, Twisted bilayer graphene aligned with hexagonal boron nitride: Anomalous hall effect and a lattice model, *Phys. Rev. Research* **1**, 033126 (2019).
- [24] Y.-H. Zhang, D. Mao, Y. Cao, P. Jarillo-Herrero, and T. Senthil, Nearly flat chern bands in moiré superlattices, *Phys. Rev. B* **99**, 075127 (2019).
- [25] N. Bultinck, S. Chatterjee, and M. P. Zaletel, Mechanism for anomalous hall ferromagnetism in twisted bilayer graphene, *Phys. Rev. Lett.* **124**, 166601 (2020).
- [26] J. Shi, J. Zhu, and A. H. MacDonald, Moiré commensurability and the quantum anomalous hall effect in twisted bilayer graphene on hexagonal boron nitride, *Phys. Rev. B* **103**, 075122 (2021).
- [27] C.-Z. Chang, J. Zhang, X. Feng, J. Shen, Z. Zhang, M. Guo, K. Li, Y. Ou, P. Wei, L.-L. Wang, Z.-Q. Ji, Y. Feng, S. Ji, X. Chen, J. Jia, X. Dai, Z. Fang, S.-C. Zhang, K. He, Y. Wang, L. Lu, X.-C. Ma, and Q.-K. Xue, Experimental observation of the quantum anomalous hall effect in a magnetic topological insulator, *Science* **340**, 167 (2013).
- [28] Y. Deng, Y. Yu, M. Z. Shi, Z. Guo, Z. Xu, J. Wang, X. H. Chen, and Y. Zhang, Quantum anomalous hall effect in intrinsic magnetic topological insulator $\text{mnbi}(2)\text{te}(4)$, *Science* **367**, 895 (2020).
- [29] M. Serlin, C. L. Tschirhart, H. Polshyn, Y. Zhang, J. Zhu, K. Watanabe, T. Taniguchi, L. Balents, and A. F. a. Young, Intrinsic quantized anomalous hall effect in a moiré heterostructure, *Science* **367**, 900 (2020).
- [30] T. Li, S. Jiang, B. Shen, Y. Zhang, L. Li, Z. Tao, T. Devakul, K. Watanabe, T. Taniguchi, L. Fu, J. Shan, and K. F. Mak, Quantum anomalous hall effect from intertwined moiré bands, *Nature* **600**, 641 (2021).
- [31] D. Litvin and W. Opechowski, Spin groups, *Physica* **76**, 538 (1974).
- [32] P. Liu, J. Li, J. Han, X. Wan, and Q. Liu, Spin-group symmetry in magnetic materials with negligible spin-orbit coupling, *Phys. Rev. X* **12**, 021016 (2022).
- [33] P.-J. Guo, Y.-W. Wei, K. Liu, Z.-X. Liu, and Z.-Y. Lu, Eightfold degenerate fermions in two dimensions, *Phys. Rev. Lett.* **127**, 176401 (2021).
- [34] Jian Yang, Zheng-Xin Liu, Chen Fang, arXiv:2105.12738.
- [35] For details see the Supplemental Material at [url], which includes Ref. [38–46].
- [36] X. Chen, D. Wang, L. Li, and B. S. Sanyal, arXiv:2104.07390 .
- [37] A. F. Izmaylov, E. N. Brothers, and G. E. Scuseria, Linear-scaling calculation of static and dynamic polarizabilities in hartree-fock and density functional theory for periodic systems, *The Journal of Chemical Physics* **125**, 224105 (2006), <https://doi.org/10.1063/1.2404667>.
- [38] A. Bouhon, G. F. Lange, and R.-J. Slager, Topological correspondence between magnetic space group representations and subdimensions, *Phys. Rev. B* **103**, 245127 (2021).
- [39] P. E. Blöchl, Projector augmented-wave method, *Phys. Rev. B* **50**, 17953 (1994).
- [40] G. Kresse and D. Joubert, From ultrasoft pseudopotentials to the projector augmented-wave method, *Phys. Rev. B* **59**, 1758 (1999).
- [41] G. Kresse and J. Furthmüller, Efficiency of ab-initio total energy calculations for metals and semiconductors using a plane-wave basis set, *Computational Materials Science* **6**, 15 (1996).
- [42] G. Kresse and J. Furthmüller, Efficient iterative schemes for ab initio total-energy calculations using a plane-wave basis set, *Phys. Rev. B* **54**, 11169 (1996).
- [43] J. P. Perdew, K. Burke, and M. Ernzerhof, Generalized gradient approximation made simple, *Phys. Rev. Lett.* **77**, 3865 (1996).
- [44] N. Marzari and D. Vanderbilt, Maximally localized generalized wannier functions for composite energy bands, *Phys. Rev. B* **56**, 12847 (1997).
- [45] I. Souza, N. Marzari, and D. Vanderbilt, Maximally localized wannier functions for entangled energy bands, *Phys. Rev. B* **65**, 035109 (2001).
- [46] Q. Wu, S. Zhang, H.-F. Song, M. Troyer, and A. A. Soluyanov, Wanniertools: An open-source software package for novel topological materials, *Computer Physics Communications* **224**, 405 (2018).

Supplemental Materials: Quantum Anomalous Hall Effect in Antiferromagnetism

Peng-Jie Guo,¹ Zheng-Xin Liu,¹ and Zhong-Yi Lu¹

¹*Department of Physics and Beijing Key Laboratory of Opto-electronic Functional Materials & Micro-nano Devices, Renmin University of China, Beijing 100872, China*

(Dated: June 8, 2022)

S1. MANIPULATION OF THE WEYL CONES

In this section, we firstly turn off SOC and investigate the number of Weyl cones when tuning the value of the staggered chemical potential μ_- . Then we analyze the symmetry constraints under which the cones can be gapped out by tuning on SOC. The constraints of the symmetry groups will be helpful in the search of AFM materials to realize the QAH effect.

A. Symmetry protected Band crossing and the Number of Weyl cones

Here we analyze the conditions for the existence of Weyl cones of the model (1) in the main text. As mentioned in the main text, the term $\Gamma_k^{12} = 0$ on the boundary of the BZ where $k_x = \pi$ or $k_y = \pi$. Therefore, on the BZ boundary the hybridization between two species of fermions C_{1k} and C_{2k} vanishes owing to the protection of their different quantum numbers under certain symmetries (see Sec.S1B for details). Consequently, if the band inversion between the C_{1k} and the C_{2k} bands takes place on the BZ boundary, then the appearance of Weyl cones will be protected by the corresponding symmetry.

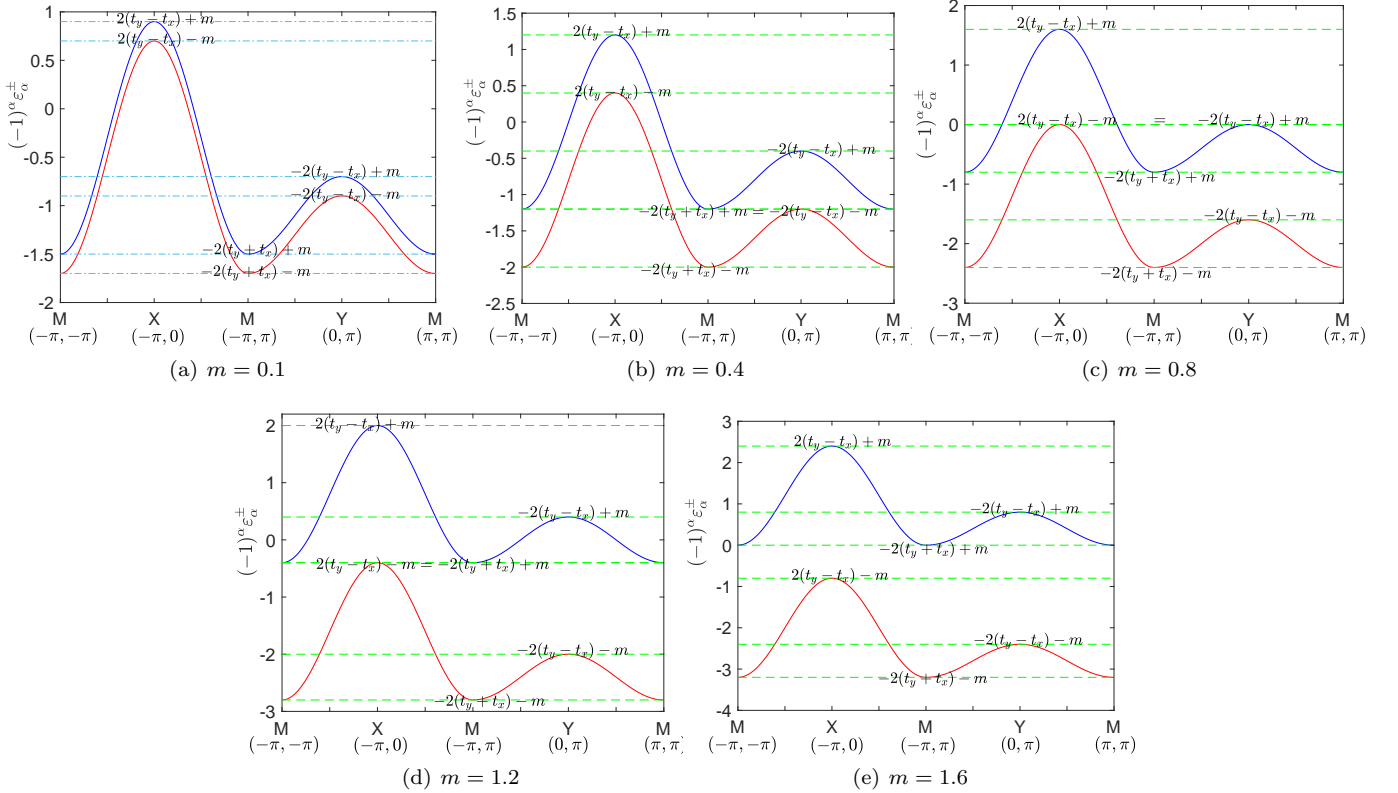


FIG. S1. The bands of $(-1)^\alpha \epsilon_\alpha^\pm(k)$ with fixed $t_y = 0.6, t_x = 0.2$ are plotted in (a)~(e) with the increasing of $m = |\mathbf{m}|$. The number of times that these bands crossed by the level μ_- determines the number of Weyl cones.

On the BZ boundary the energy spectrum is determined by $\Gamma_k^{(\alpha)}$, whose eigenvalues read

$$E_{\alpha}^{\pm}(k) = (-1)^{\alpha}(2t \cos k_x + 2t_y \cos k_y \pm m - \mu_-).$$

The band crossing can be tuned by the staggered chemical potential $\mu_- = \frac{1}{2}(\mu_1 - \mu_2)$. To see this, we define the following quantity,

$$\varepsilon_{\alpha}^{\pm}(k) = (-1)^{\alpha}(2t_x \cos k_x + 2t_y \cos k_y \pm m),$$

and consequently

$$(-1)^{\alpha} \varepsilon_{\alpha}^{\pm}(k) = 2t_x \cos k_x + 2t_y \cos k_y \pm m,$$

which is independent on α .

The number of Weyl cones can be read out from the times that the bands of $(-1)^{\alpha} \varepsilon_{\alpha}^{\pm}$ (see Fig.S1 for illustration) are crossed by the level of μ_- . In the following we analyze the dependence of the cone number and μ_- in details.

Without loss of generality, we fix t_x, t_y and assume $t_y - t_x > 0$ (the case with $t_y - t_x < 0$ is very similar). Then we vary the value of m , and look into the range of μ_- within which the number of Weyl cones is stable. It turns out that there are four different situations, as enumerated below.

- Case (1) $2(t_y - t_x) - m > -2(t_y - t_x) + m > -2(t_y - t_x) - m > -2(t_y + t_x) + m$, see Fig.1(a)
 A), if $\mu_- \in (+2(t_y - t_x) - m, +2(t_y - t_x) + m)$, μ_- cross the bands twice, there are two (1 pair of) Weyl cones;
 B), if $\mu_- \in (-2(t_y - t_x) + m, +2(t_y - t_x) - m)$, μ_- cross the bands four times, there are four (2 pairs of) Weyl cones;
 C), if $\mu_- \in (-2(t_y - t_x) - m, -2(t_y - t_x) + m)$, there are six (3 pairs of) Weyl cones;
 D), if $\mu_- \in (-2(t_y + t_x) + m, -2(t_y - t_x) - m)$, there are eight (4 pairs of) Weyl cones;
 E), if $\mu_- \in (-2(t_y + t_x) - m, -2(t_y + t_x) - m)$, there are four (2 pairs of) Weyl cones;
 F), otherwise, there are zero Weyl cone.
- Case (2) $2(t_y - t_x) - m > -2(t_y - t_x) + m > -2(t_y + t_x) + m > -2(t_y - t_x) - m$, see Fig.1(b) & 1(c)
 A), if $\mu_- \in (+2(t_y - t_x) - m, +2(t_y - t_x) + m)$, there are two (1 pair of) Weyl cones;
 B), if $\mu_- \in (-2(t_y - t_x) + m, +2(t_y - t_x) - m)$, there are four (2 pairs of) Weyl cones;
 C), if $\mu_- \in (-2(t_y + t_x) + m, -2(t_y - t_x) + m)$, there are six (3 pairs of) Weyl cones;
 D), if $\mu_- \in (-2(t_y - t_x) - m, -2(t_y + t_x) + m)$, there are two (1 pair of) Weyl cones;
 E), if $\mu_- \in (-2(t_y + t_x) - m, -2(t_y - t_x) - m)$, there are four (2 pairs of) Weyl cones;
 F), otherwise, there are zero Weyl cone.
- Case (3) $-2(t_y - t_x) + m > 2(t_y - t_x) - m > -2(t_y + t_x) + m > -2(t_y - t_x) - m$, see Fig.1(c) & 1(d)
 A), if $\mu_- \in (-2(t_y - t_x) + m, +2(t_y - t_x) + m)$, there are two (1 pair of) Weyl cones;
 B), if $\mu_- \in (+2(t_y - t_x) - m, -2(t_y - t_x) + m)$, there are four (2 pairs of) Weyl cones;
 C), if $\mu_- \in (-2(t_y + t_x) + m, +2(t_y - t_x) - m)$, there are six (3 pairs of) Weyl cones;
 D), if $\mu_- \in (-2(t_y - t_x) - m, -2(t_y + t_x) + m)$, there are two (1 pair of) Weyl cones;
 E), if $\mu_- \in (-2(t_y + t_x) - m, -2(t_y - t_x) - m)$, there are four (2 pairs of) Weyl cones;
 F), otherwise, there are zero Weyl cone.
- Case (4) $-2(t_y - t_x) + m > -2(t_y + t_x) + m > 2(t_y - t_x) - m > -2(t_y - t_x) - m$, see Fig.1(e)
 A), if $\mu_- \in (-2(t_y - t_x) + m, +2(t_y - t_x) + m)$, there are two (1 pair of) Weyl cones;
 B), if $\mu_- \in (-2(t_y + t_x) + m, -2(t_y - t_x) + m)$, there are four (2 pairs of) Weyl cones;
 C), if $\mu_- \in (-2(t_y - t_x) - m, +2(t_y - t_x) - m)$, there are two (1 pair of) Weyl cones;
 D), if $\mu_- \in (-2(t_y + t_x) - m, -2(t_y - t_x) - m)$, there are four (2 pairs of) Weyl cones;
 E), otherwise, there are zero Weyl cone.

When μ_- equals the ‘transition’ points, some pairs of cones merge into quadratic touches at the X point $(\pi, 0)$, or the Y point $(0, \pi)$, or the M point (π, π) .

Among all the above cases, when

$$|m - 2|t_y - t_x|| < |\mu_-| < m + 2|t_y - t_x|$$

is satisfied, namely, when $|m - 2|t_y - t_x|| < \mu_- < m + 2|t_y - t_x|$ or $-m - 2|t_y - t_x| < \mu_- < -|m - 2|t_y - t_x||$, there are an odd number of pairs of cones. Actually, this is also a necessary condition for the nonzero Chern number in our model.

B. Symmetry VS. the mass of the Weyl cones

In this section we study the symmetry conditions under which the Weyl cones can be gapped out. The constraints of the symmetry groups will be helpful to search for AFM materials in realizing the QAH effect.

1. Without SOC.

Firstly, we turn off SOC and analyze the quantum numbers that protect the Weyl cones. We assume that the two bases \hat{x} and \hat{y} of the lattice vectors are orthogonal such that the crystalline point group is D_{2h} generated by C_2^x, C_2^y and \mathcal{I} . Without SOC, the spin rotation symmetry operation and lattice rotation symmetry operation are unlocked, and the resultant point symmetry group is a spin point group (see the main text) which is generated by $(E||C_2^x), (E||C_2^y), (E||\mathcal{I})$ and $(C_2^\perp\mathcal{T}||\mathcal{T}), (C_2^m||E)$. Here we have adopted the notation $(g||h)$ to denote the spin point group element as a combined operation of spin rotation g and lattice operation h .

To illustrate, we analyze the boundary line (k_x, π) which is invariant under the $(E||C_2^x)$ symmetry. Under the action of $(E||C_2^x)$, the fermion C_1 on site 1 is transformed into itself, but the fermion C_2 on site 2 is shifted by a lattice constant $\mathbf{y} = a_2\hat{y}$ (here we assume a_1, a_2 are the lattice constants). Therefore, the fermion C_{1k} carries quantum number 1 of $(E||C_2^x)$, while C_{2k} carries a quantum number $e^{-i\pi} = -1$ remembering that $k_y = \pi$. These different quantum numbers protect the band crossing points, i.e. the Weyl cones, from being gapped out. Since (E, \mathcal{I}) is always a symmetry, the symmetry that providing the quantum numbers can also be chosen as $(E||M_x) = (E||C_2^x) \times (E, \mathcal{I})$. Similarly, the Weyl cones on the (π, k_y) boundary line, if exist, are protected by the quantum numbers of the $(E||C_2^y)$ or $(E||M_y)$ symmetry.

However, the Weyl cones may be robust against being gapped out even with the absence of the symmetry elements (such as $(E||C_2^x)$) which provide the quantum numbers. For instance, if the crystalline symmetry is lowered by applying shear strain, the Weyl cones will still be stable.

Actually, the robustness of the cones are owing to the combined anti-unitary symmetry operation $(C_2^\perp\mathcal{T}||\mathcal{IT}) = (E||\mathcal{I}) \times (C_2^\perp\mathcal{T}||\mathcal{T})$. This symmetry $(C_2^\perp\mathcal{T}||\mathcal{IT})$ is always there since the inversion symmetry $(E||\mathcal{I})$ is preserved as we require and that the AFM order we are considering is collinear such that $(C_2^\perp\mathcal{T}||\mathcal{T})$ is a symmetry. This spin point group symmetry operation $(C_2^\perp\mathcal{T}||\mathcal{IT})$ differs with the familiar space-time inversion operation $(\mathcal{T}||\mathcal{IT})$ (usually denoted as \mathcal{IT} for simplicity) by a pure spin rotation $(C_2^\perp||E)$. Notice that the space-time inversion symmetry $(\mathcal{T}||\mathcal{IT})$ is a symmetry of momentum points in the whole BZ, and it ensures that the Berry curvature is vanishing for all momentum point k whose energy spectrum is gapped. Furthermore, in the presence of $(\mathcal{T}||\mathcal{IT})$ symmetry, the Berry phase for a closed loop is quantized to π or 0: it is equal to π if it encloses an odd number of Weyl cones and equals to zero if it encloses an even number of Weyl cones. On the other hand, the spin rotation $(C_2^\perp||E)$ does not act on the momentum k and does not change the Berry curvature. Consequently, the above results for the symmetry $(\mathcal{T}||\mathcal{IT})$ are also valid for the spin-point symmetry $(C_2^\perp\mathcal{T}||\mathcal{IT})$.

Since $(C_2^\perp\mathcal{T}||\mathcal{IT})$ ensures that the Berry phase of any loop in the BZ is quantized to π or 0 (here we assume that the spectrum on the loop is fully gapped), the Weyl cones cannot be solely gapped out. Resultantly, under perturbations (such as shear strain) preserving the $(C_2^\perp\mathcal{T}||\mathcal{IT})$ symmetry, the Weyl cones adiabatically shift their positions. The number of cones can be reduced in pair if two cones move toward each other, then merge and finally open a gap. So if the $(C_2^\perp\mathcal{T}||\mathcal{IT})$ symmetry preserving perturbations are not strong, then the Weyl cones remain robust.

2. With SOC.

When SOC is present, the physical symmetry of a magnetically ordered system is described by a magnetic group where the lattice rotation operations are locked with the corresponding spin rotations.

In-plane AFM order. Firstly we consider in-plane AFM order. Without loss of generality, we assume that $\mathbf{m} \parallel \hat{y}$. In this case, $(C_2^y||C_2^y)$ is a symmetry operation if the crystalline point group contains C_2^y . Since $(C_2^y||C_2^y)$ has quantum numbers $\pm i$, these quantum numbers can still protect the band crossing on the line (π, k_y) (whose little co-group contains the symmetry operation $(C_2^y||C_2^y)$) from being gapped out. In our model, the Hamiltonian on the line (π, k_y) reads

$$H_k = C_{1k}^\dagger \left[-4i\boldsymbol{\lambda} \cdot \boldsymbol{\sigma} \sin \frac{k_y}{2} \right] C_{2k} + \sum_{\alpha} (-1)^{\alpha} C_{\alpha k}^\dagger \left[2t_y \cos k_y - 2t_x + \mathbf{m} \cdot \boldsymbol{\sigma} - \mu_- \right] C_{\alpha k}.$$

Since the $(C_2^y||C_2^y)$ symmetry is a physical requirement, only λ_x and λ_z components are symmetry allowed: the lattice part $(E||C_2^y)$ transforms $\boldsymbol{\lambda}^{d_1}$ to $\boldsymbol{\lambda}^{d_2} = -\boldsymbol{\lambda}^{d_1}$ and the spin part $(C_2^y||E)$ send $-\lambda_{x,z}^{d_1}$ back to $\lambda_{x,z}^{d_1}$. In this case, the Weyl

cons on the line (π, k_y) , if exist, are still robust even if the C_{1k} and C_{2k} fermions are indeed hybridized owing to the SOC.

Similarly, the quantum numbers $\pm i$ of $(C_2^y || M_y) = (C_2^y || C_2^y) \times (E || \mathcal{I})$ can protect the Weyl cones on the line (k_x, π) from being gapped out (see Fig. S2(a)). Notice that the symmetry $(C_2^y || M_y)$ is preserved as long as the SOC term λ lies in the xz -plane such that $\mathbf{m} \cdot \boldsymbol{\lambda} = 0$.

Therefore, if $\mathbf{m} \cdot \boldsymbol{\lambda} = 0$ then the Weyl cones on the BZ boundary are still robust owing to the protection of quantum numbers of either $(C_2^y || C_2^y)$ or $(C_2^y || M_y)$. This result indicates that if the AFM order is parallel to an in-plane C_2 axis, then the Weyl cones resulting from band inversion will remain robust and QAH effect cannot be realized.

If $\boldsymbol{\lambda} \cdot \mathbf{m} \neq 0$, then all the Weyl cones obtain a mass, which results in a QAH insulator. If both $\boldsymbol{\lambda}$ and \mathbf{m} are parallel to \hat{y} , then the symmetry group of the model reads $2'/m' = \{E, \mathcal{I}, C_2^x \mathcal{T}, M_x \mathcal{T}\}$. In this case, the crystalline point group is C_{2h} . If $\boldsymbol{\lambda}$ is neither perpendicular nor parallel to \mathbf{m} , then the symmetry group of the model reduces to $\bar{1} = \{E, \mathcal{I}\}$. Therefore, QAH insulators can be realized in in-plane AFM ordered systems if the lattice structure is either triclinic or monoclinic.

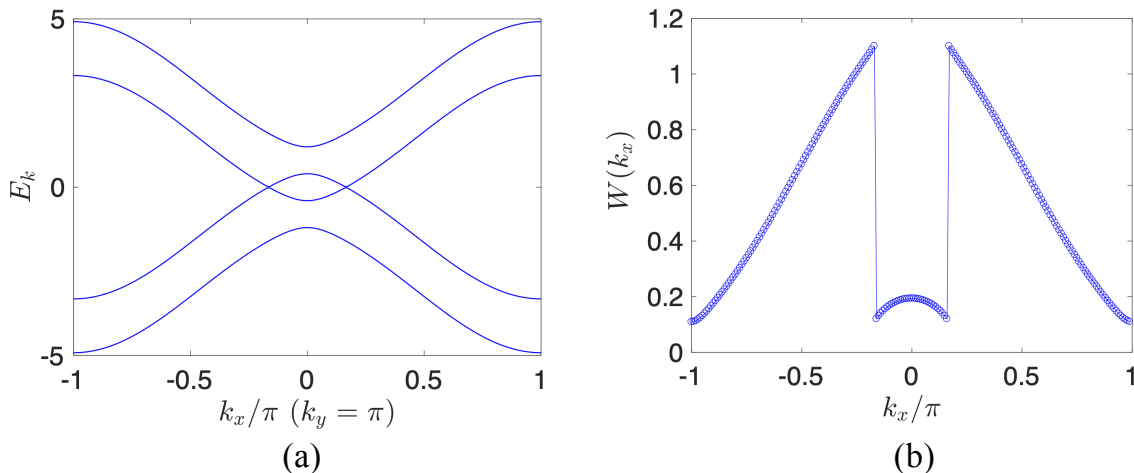


FIG. S2. (a) The Weyl cones are robust against SOC when $\lambda_y \neq 0, \lambda_z \neq 0$ and $\lambda_x = 0$ given that $\mathbf{m} \parallel \hat{x}$. (b) The 1D chain with given k_x is not topological since the Berry phase $W(k_x)$ (see Eq. (S3)) is not quantized.

Out-of-plane AMF order. Then we consider the case where the AFM order is perpendicular to the lattice plane, namely $\mathbf{m} \parallel \hat{z}$. In this case, the QAH effect can be realized if $\lambda_z \neq 0$.

If $\boldsymbol{\lambda} \parallel \hat{z}$, then the model has a higher symmetry which is described by the magnetic point group $m'm'm = \{E, C_2^x \mathcal{T}, C_2^y \mathcal{T}, C_2^z, \mathcal{I}, M_x \mathcal{T}, M_y \mathcal{T}, M_z\}$. Therefore, QAH insulator can be realized in AFM materials with crystalline point group D_{2h} generated by C_2^x, C_2^y and \mathcal{I} .

The above symmetry conditions can be released. For instance, if $\boldsymbol{\lambda}$ is deviated from \hat{z} or if the lattice axis \hat{a} and \hat{b} are not orthogonal, then the magnetic point group can be lowered to $2'/m' = \{E, \mathcal{I}, C_2^x \mathcal{T}, M_x \mathcal{T}\}$ or $\bar{1} = \{E, \mathcal{I}\}$. Therefore, if the magnetic order is perpendicular to the lattice plane, QAH insulators can be possibly found in AFM materials having triclinic, monoclinic, or orthogonal lattice structure.

If the unit cell contains more than two magnetic sites, the resultant Chern number maybe greater than one[1].

It should be mentioned that our discussion is restricted to the mechanism that the Weyl cones come from the inversion of bands with different quantum numbers. The Weyl cones may also arise from symmetry protection or from critical points[2], in which cases the above symmetry analysis is no-longer applicable.

S2. CHERN NUMBER AND EDGE STATES

When the two Weyl cones on the boundary (k_x, π) are gapped out, one obtains a QAH insulator because the Chern number is nonzero. Here we briefly summarize the method in the computation of the Chern number in discretized momentum space.

Firstly we calculate the Berry connection $A_i(k) \in [-\pi, \pi)$ with $i = x, y$ and $k = (k_x, k_y)$,

$$A_i(k) = \text{Im}(\log \det \mathcal{O}_i(k)), \quad (\text{S1})$$

where Im means the imaginary part and $O_i(k)$ is a 2 by 2 matrix defined from the following overlap

$$[O_i(k)]^{ab} = \langle \phi_a(k) | \phi_b(k + \delta k_i) \rangle,$$

where $a, b = 1, 2$ are the indices of the occupied bands, δk_i is the step length of the discretized momenta along the i -direction, and $|\phi_a(k)\rangle$ are eigenvectors of H_k with

$$H_k |\phi_a(k)\rangle = E_k |\phi_a(k)\rangle.$$

As Γ_k^{12} contains the variables $\frac{k_x}{2}, \frac{k_y}{2}$, the Hamiltonian is not periodic in the first BZ and the same for their eigenstates. Nevertheless, the Chern number can still be computed, as long as both $|\phi(k_x, -\pi)\rangle$ and $|\phi(k_x, \pi)\rangle$, and similarly both $|\phi(-\pi, k_y)\rangle$ and $|\phi(\pi, k_y)\rangle$ are kept. With these states, the following matrices are defined,

$$\begin{aligned} [\mathcal{O}_x(\pi - \delta k_x, k_y)]^{ab} &= \langle \phi_a(\pi - \delta k_x, k_y) | \phi_b(\pi, k_y) \rangle, & [\mathcal{O}_y(\pi, k_y)]^{ab} &= \langle \phi_a(\pi, k_y) | \phi_b(\pi, k_y + \delta k_y) \rangle, \\ [\mathcal{O}_y(k_x, \pi - \delta k_y)]^{ab} &= \langle \phi_a(k_x, \pi - \delta k_y) | \phi_b(k_x, \pi) \rangle, & [\mathcal{O}_x(k_x, \pi)]^{ab} &= \langle \phi_a(k_x, \pi) | \phi_b(k_x + \delta k_x, \pi) \rangle. \end{aligned}$$

Hence $A_x(\pi - \delta k_x, k_y)$, $A_y(\pi, k_y)$ and $A_y(k_x, \pi - \delta k_y)$, $A_x(k_x, \pi)$ are obtained from (S1).

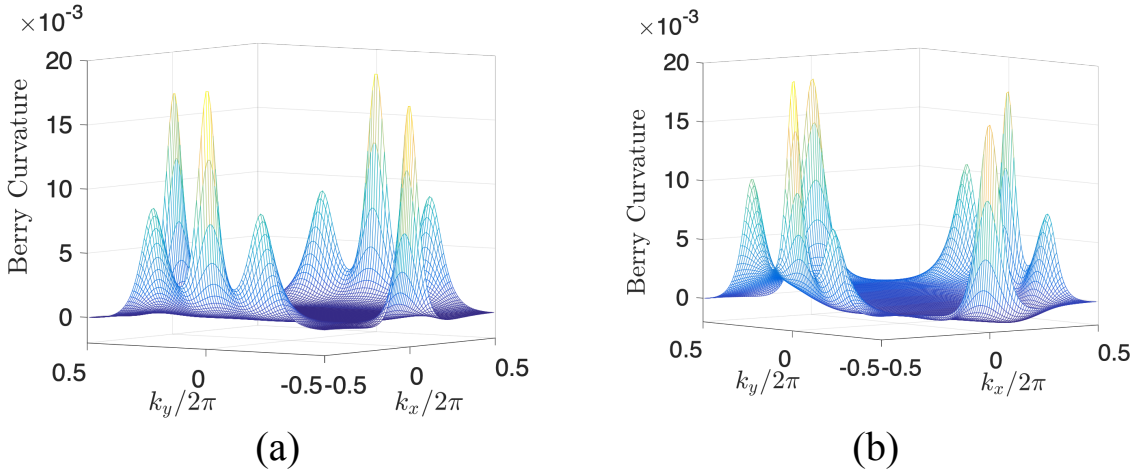


FIG. S3. Pictures of Berry curvature calculated in two different conventions both resulting in a Chern number $C = 1$. (a) With the original \mathbf{d}_i , the Berry curvature preserves the inversion symmetry; (b) With the transformation $\mathbf{d}_i \rightarrow \mathbf{d}_i - \frac{1}{2}(\mathbf{x} + \mathbf{y})$, the Berry curvature no longer preserves the inversion symmetry.

Then we calculate the Berry curvature $F(k)$ for $k_x \in [-\pi, \pi]$, $k_y \in [-\pi, \pi]$,

$$F(k) = [A_x(k) + A_y(k + \delta k_x) - A_x(k + \delta k_y) - A_y(k)] \text{mod } 2\pi.$$

When k_x, k_y are fine-grained, $F_{ij}(k)$ should be a small number. However, owing to a random gauge choice of the numerically obtained $|\phi_j(k)\rangle$, sometimes $F_{ij}(k)$ may be as big as close to $2\pi N$, $N \in \mathbb{Z}$, so we adopt mod 2π to guarantee that $F_{ij}(k)$ is indeed small (See Fig. S3).

Finally, we obtain the Chern number from the summation of F over the BZ,

$$C = \frac{1}{2\pi} \sum_{k_x \in [-\pi, \pi]} \sum_{k_y \in [-\pi, \pi]} F(k_x, k_y). \quad (\text{S2})$$

Above we illustrate that the Chern number can be calculated regardless that the Hamiltonian is not periodic in the first BZ. The reason is that the Hamiltonian can be made periodic in the first BZ under a nonsingular unitary transformation which does not change the Chern number. This can be done by adopting another convention to coordinate the lattice sites within a unit cell. When shifting $\mathbf{d}_i \rightarrow \mathbf{d}_i - \frac{1}{2}(\mathbf{x} + \mathbf{y})$, the new Hamiltonian no longer contains $\frac{k_x}{2}, \frac{k_y}{2}$, thus are periodic in the first BZ. In this case, one can simply replace $|\phi_a(\pi, k_y)\rangle$ by $|\phi_a(-\pi, k_y)\rangle$ and replace $|\phi_a(k_x, \pi)\rangle$ by $|\phi_a(k_x, -\pi)\rangle$. Accordingly the formulas for $A_x(\pi - \delta k_x, k_y)$, $A_y(\pi, k_y) = A_y(-\pi, k_y)$ and $A_y(k_x, \pi - \delta k_y)$, $A_x(k_x, \pi) = A_x(k_x, -\pi)$ will be modified, but the formula (S2) for computing the Chern number remains unchanged.

In momentum space, the transformation $\mathbf{d}_i \rightarrow \mathbf{d}_i - \frac{1}{2}(\mathbf{x} + \mathbf{y})$ is k -dependent, consequently the Berry curvature is affected (the Chern number remains the same). For instance, the Berry curvature is inversion symmetric in the first

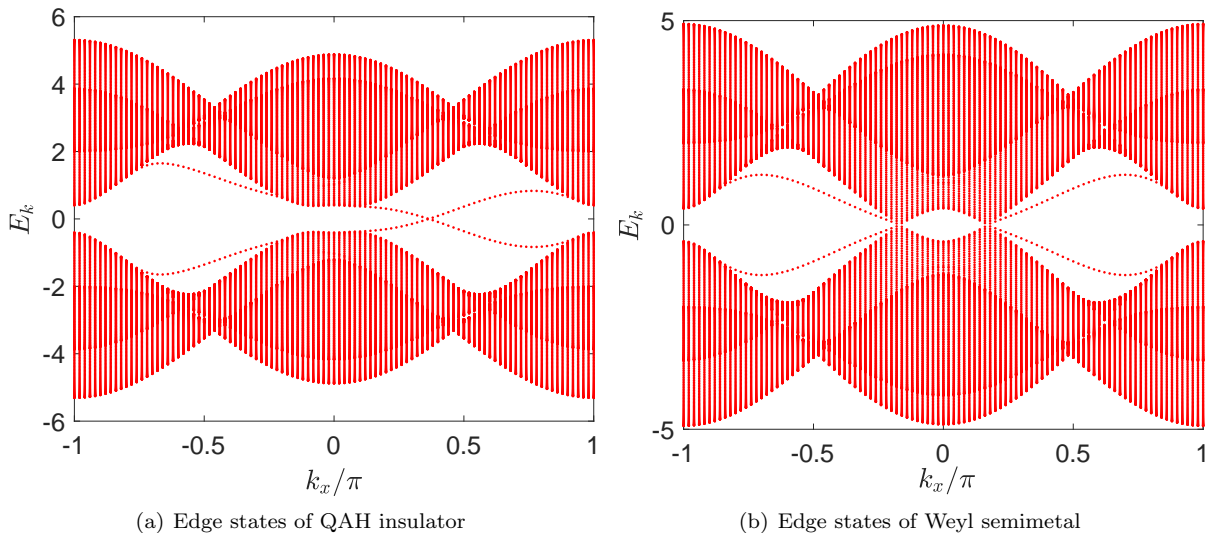


FIG. S4. Edge states of (a) QAH insulator with $\lambda_x = 0.5$, (b) Weyl semimetal with $\lambda_x = 0$.

convention (see Fig. S3 (a)), but after the transformation $\mathbf{d}_i \rightarrow \mathbf{d}_i - \frac{1}{2}(\mathbf{x} + \mathbf{y})$, the resultant Berry curvature is no longer inversion symmetric (see Fig. S3 (b)).

The nontrivial bulk Chern number is further verified by the existence of chiral edge states. If one adopt the cylinder geometry with periodic boundary condition along the x -direction (such that k_x is still a good quantum number) and open boundary condition along the y -direction, there will be two branches of chiral edge states, as shown in Fig. S4(a).

In the following we discuss the edge states of the Weyl semimetal with $\lambda_x = 0$. Suppose that the parameters are chosen such that there is one pair of Weyl cones in the BZ boundary line (k_x, π) . We still adopt cylinder geometry as before. Since k_x is a good quantum number, one can consider the Hamiltonian with fixed k_x as a 1D chain. If the 1D chain has zero energy edge states, then there will exist zero-energy edge states on the open boundary of the 2D cylinder.

Since the zero edge mode of 1D chain requires a topological invariant or π -quantization of the Berry phase. Here we calculate the Zak phase of the 1D chain with given k_x ,

$$W(k_x) = \left[\frac{1}{\pi} \sum_{k_y \in [-\pi, \pi]} A_y(k_x, k_y) \right] \text{mod } 2, \quad (\text{S3})$$

where $A_y(k_x, k_y)$ is defined in Eq. (S1).

Since quantization condition requires that the Hamiltonian is periodic in the 1D momentum space $k_x \in [-\pi, \pi]$, we adopt the single valued Hamiltonian after the transformation $\mathbf{d}_i \rightarrow \mathbf{d}_i - \frac{1}{2}(\mathbf{x} + \mathbf{y})$. The Berry phase indeed jumps by π when k_x passes the position of the Weyl cones, however the quantity $W(k_x)$ in (S3) is not an integer for most k_x (see Fig. S2(b)). Therefore, we conclude that the invariant is absent and consequently no zero-energy edge modes are protected. However, the jump of the Berry phase at the position of the Weyl cones indicates that the situations are indeed different inside the two Weyl cones and outside the Weyl cones. As shown in Fig. S4(b), the dispersive middle gap edge states are found outside the cones but are absent inside the cones.

S3. DETAILS ABOUT THE FIRST PRINCIPLE CALCULATIONS

The electronic structures of a monolayer CrO were studied with the projector augmented wave method[3, 4] as implemented in the VASP package[5, 6]. The Perdew-Burke-Ernzerhof exchange-correlation functional at the generalized gradient approximation level was adopted to describe the interaction between the ionic cores and the valence electrons[7]. For the electronic correlation in the d orbitals of Cr^{2+} , we adopted the Hubbard U formalism. The kinetic energy cutoff of the plane-wave basis was set to 700 eV and a $20 \times 20 \times 1$ was adopted for the k -point mesh. The Gaussian smearing method with a width of 0.01 eV was utilized for the Fermi surface broadening. Both cell parameters and internal atomic positions were fully relaxed until the forces on all atoms were smaller than 0.001 eV/Å. The calculated lattice parameters were 1.4 percent less than the previous values[8]. A 20 Å vacuum layer was

used to avoid the residual interaction between adjacent layers. The Berry curvature of monolayer CrO was calculated by using the Wannier90 package[9, 10]. The topological invariants and the chiral edge states of monolayer CrO were studied by WannierTools package[11].

-
- [1] A. Bouhon, G. F. Lange, and R.-J. Slager, Topological correspondence between magnetic space group representations and subdimensions, *Phys. Rev. B* **103**, 245127 (2021).
 - [2] K. Jiang, S. Zhou, X. Dai, and Z. Wang, Antiferromagnetic chern insulators in noncentrosymmetric systems, *Phys. Rev. Lett.* **120**, 157205 (2018).
 - [3] P. E. Blöchl, Projector augmented-wave method, *Phys. Rev. B* **50**, 17953 (1994).
 - [4] G. Kresse and D. Joubert, From ultrasoft pseudopotentials to the projector augmented-wave method, *Phys. Rev. B* **59**, 1758 (1999).
 - [5] G. Kresse and J. Furthmüller, Efficiency of ab-initio total energy calculations for metals and semiconductors using a plane-wave basis set, *Computational Materials Science* **6**, 15 (1996).
 - [6] G. Kresse and J. Furthmüller, Efficient iterative schemes for ab initio total-energy calculations using a plane-wave basis set, *Phys. Rev. B* **54**, 11169 (1996).
 - [7] J. P. Perdew, K. Burke, and M. Ernzerhof, Generalized gradient approximation made simple, *Phys. Rev. Lett.* **77**, 3865 (1996).
 - [8] X. Chen, D. Wang, L. Li, and B. S. Sanyal, ArXiv: **2104**, 07390 (2021).
 - [9] N. Marzari and D. Vanderbilt, Maximally localized generalized wannier functions for composite energy bands, *Phys. Rev. B* **56**, 12847 (1997).
 - [10] I. Souza, N. Marzari, and D. Vanderbilt, Maximally localized wannier functions for entangled energy bands, *Phys. Rev. B* **65**, 035109 (2001).
 - [11] Q. Wu, S. Zhang, H.-F. Song, M. Troyer, and A. A. Soluyanov, Wanniertools: An open-source software package for novel topological materials, *Computer Physics Communications* **224**, 405 (2018).